Stark effect and dipole moments of the ammonia dimer in different vibration–rotation–tunneling states

Gina Cotti,[a] Harold Linnartz, and W. Leo Meerts
Department of Molecular and Laser Physics, University of Nijmegen, Toernooiveld, 6525 ED Nijmegen, The Netherlands

Ad van der Avoird and Edgar H. T. Olthof
Institute of Theoretical Chemistry, University of Nijmegen, Toernooiveld, 6525 ED Nijmegen, The Netherlands

In this paper we present Stark measurements on the $G:K=-1$ vibration–rotation–tunneling (VRT) transition, band origin 747.2 GHz, of the ammonia dimer. The observed splitting pattern and selection rules can be explained by considering the G_{36} and G_{144} symmetries of the inversion states involved, and almost complete mixing of these states by the applied electric field. The absolute values of the electric dipole moments of the ground and excited state are determined to be 0.763(15) and 0.365(10) D, respectively. From the theoretical analysis and the observed selection rules it is possible to establish that the dipole moments of the two interchange states must have opposite sign. The theoretical calculations are in good agreement with the experimental results: The calculated dipole moments are -0.74 D for the lower and $+0.35$ D for the higher state. Our results, in combination with the earlier dipole measurements on the $G:K=0$ ground state and the $G:K=1$ transition with band origin 486.8 GHz, confirm that the ammonia dimer is highly nonrigid. Its relatively small and strongly K-dependent dipole moment, which changes sign upon far-infrared excitation, originates from the difference in dynamical behavior of ortho and para NH_3. © *1996 American Institute of Physics.* [S0021-9606(96)03409-8]

I. INTRODUCTION

Recently it has become clear that the seemingly contradictory experimental data on the ammonia dimer are the consequence of the dynamical character of this complex.[1–5] The initial results of Nelson *et al.*[6] in 1985, which showed that $(NH_3)_2$ prefers a nearly antiparallel structure for the $G:K=0$ state, rather than the expected linear hydrogen bonded configuration, could be explained as partly due to an averaging effect in a highly nonrigid molecule.[3] Within the same model also the results for $(ND_3)_2$, which at first view suggested a rigid structure,[1,7] could be explained. Both from experimental[8–10] and theoretical[3,11,12] evidence it was concluded that the barrier for interchange motion is very low and consequently that tunneling can easily occur.

Furthermore, it was found that the monomer umbrella inversion is only partially quenched in the complex.[2,8,9,13] The appropriate symmetry group had to be extended from G_{36} to G_{144}. Within this new group all known microwave and far-infrared data could be (re)assigned and recently also the infrared spectrum around 1000 cm^{-1} could be interpreted.[10] Using Stark spectroscopy in a jet expansion on the far-infrared transition with band origin 486.8 GHz, Linnartz *et al.*[14] determined the electric dipole moment for the lowest $G:K=1$ state to be 0.10 D. The theoretical value[3] was in good agreement with this value and illustrates that the average $(NH_3)_2$ structure for this state is indeed nearly antiparallel. The remarkable variation of the dipole with K

($\mu_{G:K=0}=0.74$ D,[6,7] $\mu_{G:K=1}=0.10$ D) proved, once again, that the interchange barrier in the potential surface is very low.

In this paper we present Stark measurements on the far-infrared transition between the lowest $G:K=-1$ states, with band origin 747.2 GHz. We found that the observed selection rules cannot be explained by the standard treatment of the Stark effect in a (nearly) symmetric rotor. We had to use the symmetry of the vibration–rotation–tunneling (VRT) states of the ammonia dimer in rather great detail, see Sec. III. From this theoretical analysis it follows that not only the dipole values of both the ground and excited VRT state are determined experimentally, but that also the relative sign of these dipole moments can be extracted from the measurements, see Sec. IV A. This is similar to the determination of the relative sign of the dipole moments in two electronic states of a molecule from field-induced optical spectra.[15] In Sec. IV B the experimental results are compared with theoretical calculations and in Sec. V it is discussed which new information on the ammonia dimer they provide.

II. EXPERIMENT

The measurements were performed with the Nijmegen tunable far-infrared sideband spectrometer, that was described in detail before.[16] For the frequencies involved, sidebands of the HCOOH and CH$_3$I emissions at 692 951.4 and 670 463.0 MHz and klystrons in the range of 74.2 to 76.5 GHz are used. The ammonia complexes are generated by expanding a mixture of approximately 3% NH_3 in Ar through a 4 cm×75 μm slit nozzle expansion into a vacuum chamber

---

[a] Permanent address: Dip. di chimica "G. Ciamician," Università degli studi di Bologna, via Selmi 2, 40126 Bologna, Italy.

that is maintained at a pressure of 0.1 mbar during jet operation by a roots pump system. The Stark setup is the same as described in Ref. 14; two metal plates ($15 \times 5 \times 4.1$ cm) are positioned on both sides of the nozzle parallel to the slit, 5 cm apart. The electric field is applied by a stabilized power supply. Due to the relatively large background pressure, it is not possible to apply larger field strengths than about 40 V/cm without breakdowns of the electric field. The relative error in the applied electric field strength is considered to be about 2.5%, calculated with "Simion,"[14] and it is mainly caused by the inhomogeneities of the electric field which arise from the relatively unfavorable dimensions of the Stark plates and the presence of the nozzle between the plates.

The far-infrared beam passes the jet expansion and is focussed onto an InSb hot electron bolometer. The radiation is frequency modulated and the detector output is monitored at twice this frequency. The sidebands have both parallel and perpendicular polarizations with respect to the electric field, i.e., both $\Delta M = 0$ and $\Delta M = \pm 1$ transitions are observed. The ratio between parallel and perpendicular sideband power is approximately 3:2. This depends mainly on the far-infrared emission and on the alignment of the Michelson polarizer used to discriminate between fundamental and sideband radiation.[16] With a polarizer placed just in front of the vacuum machine, the actual polarization, i.e., the nature of the transition, can be determined unambiguously.

The frequencies of the $Q(1)$ transitions around 747 GHz (see below) lie just 5 GHz away from the center frequency of a moderately strong water absorption around 752 GHz (transition $2_{0,2} \rightarrow 2_{1,1}$). At atmospheric pressure this water absorption is broadened to several GHz, causing a serious decrease of the maximum obtainable sideband power. However, the power was still strong enough to obtain an acceptable signal to noise ratio for the Q transitions.

The reported Stark splittings are the average values obtained from different measurements. Although the error in the absolute frequency measurements is about ± 500 kHz, due to the large gain profile of the free running FIR laser emission, the uncertainty in the experimental splittings is one order of magnitude smaller. This is because the short time stability of the laser during the scan of the spectrum is much higher. The error in the splittings, approximately 50 kHz, is therefore mainly determined by the remaining short term frequency drift of the far-infrared laser.

III. THEORY

In order to interpret the measured Stark spectra one has to consider the permutation-inversion symmetry of the VRT states of the ammonia dimer. These symmetry aspects are extensively treated in Refs. 2, 3, and 13. Here, we present only a brief outline, necessary to understand the Stark splittings of the levels and the selection rules.

A. Symmetry of the eigenstates

For the ammonia dimer with rigid monomers the permutation-inversion group is G_{36}. It follows from this symmetry that the ammonia dimer can have a permanent dipole moment only in the states of E_3, E_4, and G symmetry.[2] In the states that belong to the A_1, A_2, A_3, A_4, E_1, and E_2 irreducible representations of G_{36}, the dipole moment must vanish when averaged over the internal motions of the dimer. In reality, however, the well known inversion tunneling of the ammonia monomers, although hindered, is not completely quenched in the dimer. The VRT levels show further splittings and the appropriate permutation-inversion group is G_{144} rather than G_{36}. These splittings have been explicitly measured by Loeser *et al.*[8]

The adaptation of the VRT states to the group G_{144} is treated by Olthof *et al.*[13] The splittings associated with the hindered inversion tunneling of the monomers in the ammonia dimer were quantitatively calculated by these authors. It turned out that the magnitude of these splittings depends very sensitively on the symmetry of the VRT states and on the (approximate) quantum number K. This quantum number (which is called Ω in Ref. 2) is the component of the total angular momentum $\mathbf{J}$ along the dimer bond axis $\mathbf{R}$ (which is the vector that connects the centers of mass of the monomers A and B). Basis functions with different K are just slightly mixed by the weak Coriolis coupling between the internal angular momenta $\mathbf{j}_A$ and $\mathbf{j}_B$ of the monomers and the overall angular momentum $\mathbf{J}$. The calculations in Ref. 13, which are based on the VRT states and the semiempirical potential derived in Ref. 3, yield splittings in very good agreement with the measurements[8] and it could be explained why these splittings vary over several orders of magnitude for the different symmetries and $|K| = 0$, 1 and 2.

The VRT states of the ammonia dimer with inverting monomers that are adapted to the symmetry group G_{144} cannot have a permanent dipole moment. This follows easily, since the operator E^* that inverts the whole system is contained in G_{144} and, hence, the VRT states must have a definite parity with respect to E^*, while the dipole moment operator has of course odd parity. So the ammonia dimer in fact has no permanent dipole moment. What is measured is the off-diagonal matrix element of the dipole operator between the states with different $+/-$ parity. This matrix element can be derived from the observed Stark splittings of the $+/-$ doublets which, for zero field, are slightly split already by the hindered inversion tunneling of the ammonia monomers. In principle, this is comparable with the well known case of the free ammonia monomer, where the eigenstates are even or odd with respect to the umbrella inversion and the "dipole moment" of the ammonia molecule is in fact the off-diagonal dipole matrix element between the $+/-$ states. Also in other cases, e.g., for Λ- or l-type doublets, one has a similar situation.

Still, in the ammonia dimer with all its internal motions (in particular the monomer interchange motion) that affect the average dipole moment and the hindered umbrella inversion of the monomers, the situation is considerably more complex. To assign the Stark spectrum we must use the full symmetry group and derive how the off-diagonal dipole matrix element between the $+/-$ states adapted to G_{144} is related to the permanent dipole moment (i.e., the dipole expectation value) of a VRT state adapted to G_{36}. We treat in

particular the G states of G_{36}, since the present experiments and also all previous measurements of the dipole moment[6,7,14] refer to these states. These G states are split into $G_1^\pm$ and $G_2^\pm$ doublets of G_{144} by the hindered umbrella inversion tunnelings; only the $G_2^\pm$ doublets can be observed for the protonated ammonia dimer, since the $G_1^\pm$ states have zero spin statistical weight. For $K=0$ the $G_2^\pm$ splittings are relatively large (3.3 and 2.4 GHz for the lowest states). For $K=\pm1$ they are smaller by 3 to 4 orders of magnitude and proportional to $J(J+1)$, since they enter indirectly through Coriolis coupling.[13] In most cases the G_2^+ levels are higher in energy than the G_2^- levels for even J, while for odd J the order is reversed. The present measurements concern the $G_2^\pm$ levels with $|K|=1$ which are labeled (5,6) and (13,14) by Loeser *et al.*[8] The energy ordering of the $G_2^\pm$ levels (5,6) is different from normal; the origin of this anomaly is also explained by Olthof *et al.*[13] Note that the parity of all $G_2^\pm$ states must be reversed with respect to the assignment given by Loeser *et al.*[8] It was not possible on the basis of the experimental spectrum alone to assign the absolute parity of these levels, only their relative parity is determined by the selection rules. In the present paper we follow Ref. 13.

The wave functions of the $G_2^\pm$ states adapted to G_{144} can be written as

$$|i,G_2^\pm,JKM\rangle = \tfrac{1}{2}(E\pm E^*)[E-(23)]|i,G,K\rangle|JKM\rangle|{++}\rangle, \tag{1}$$

where $|i,G,K\rangle$ denotes that part of the ith eigenfunction of G symmetry in G_{36} that depends on the six internal coordinates of the dimer with rigid monomers, $|JKM\rangle$ is an overall rotation function and $|{++}\rangle = |f_+(\rho_A)f_+(\rho_B)\rangle$ is a function of the umbrella angles ρ_A and ρ_B of the monomers. The permutation (23) interchanges the protons 2 and 3 of monomer A and thereby inverts this monomer: $(23)|{++}\rangle = |{-+}\rangle$, while the overall inversion operator E^* inverts both monomers: $E^*|{++}\rangle = |{--}\rangle$. But these operators have some other effects on the wave functions as well, see Table II of Ref. 13. The internal functions can be expanded in basis functions

$$|i,G,K\rangle = \sum_{j_A k_A j_B k_B jn} c^{(iGK)}_{j_A k_A j_B k_B jn}|j_A k_A j_B k_B jKn\rangle, \tag{2}$$

which are products of the symmetric top functions of the monomers A and B with quantum numbers j_A, k_A, and j_B, k_B, coupled to total internal angular momentum j and projection K on the dimer axis, and multiplied by radial basis functions labeled by n, see Refs. 2 and 3. For the G states of G_{36} with monomer A as the ortho monomer, and monomer B as the para monomer, the values of k_A and k_B must obey the rule: $k_A=0$ (modulo 3) and $k_B=\pm1$ (modulo 3). The rotation functions $|JKM\rangle$ are normalized symmetric top functions $D^{(J)*}_{MK}$ with functions $D^{(J)}_{MK}$ that are elements of Wigner D matrices.[17] For the umbrella coordinates we start with the function $|{++}\rangle$ that corresponds to both monomers having their umbrella up; the operators (23) and E^* take care of the inversion of the umbrellas.

As mentioned earlier, we assume that K is a good quantum number. Although the slight mixing of functions with

different K induced by the weak Coriolis coupling is essential to calculate the very small zero-field splittings of the $G_2^\pm$ states with $K=\pm1$, this mixing will hardly affect the dipole matrix elements over the eigenstates $|i,G_2^\pm,JKM\rangle$ which we discuss below. We have included K also in the internal part $|i,G,K\rangle$ of the wave function, because it was found in Refs. 2 and 3 that the states with different K have very different internal wave functions.

It follows from the theory in Refs. 3 and 13 that the G states in G_{36} and, hence, also the $G_2^\pm$ states in G_{144}, are characterized by a quantum number K *including its sign*. The sign of K is not determined in an absolute sense, but relative to the sign of the quantum number k_B of the para monomer, which we choose to be monomer B and to have $k_B=-1$ (modulo 3). The G states labeled (3,4) and (9,10) by Loeser *et al.*[8] correspond to $K=+1$, while the states labeled (5,6) and (13,14) to which our measurements refer correspond to $K=-1$. The total wave function of the ammonia dimer including the nuclear spin functions will contain functions with $+K$ and $-K$, in combination with $k_B=\pm1$ (modulo 3) and functions in which A is the para monomer. But, since the electric dipole operator does not couple the different nuclear spin functions, we may limit ourselves here to a single value of K for each state of G symmetry. The same holds for the states of E_1 and E_2 symmetry, whereas the states of A_1, A_2, A_3, A_4, E_3, and E_4 symmetry combine the functions with $+K$ and $-K$ with equal weights.[13] This property of the G states turns out to be crucial for the selection rules of the dipole transitions that we discuss below. It will be shown that these differ from the standard rigid rotor selection rules observed in (nearly) symmetric tops.

B. Stark splitting of the levels

The derivation of the dipole coupling matrix elements between the wave functions from Eq. (1) is given in the Appendix. When calculating the Stark splitting of a given doublet $|i,G_2^\pm,JKM\rangle$, derived from a single state $|i,G,K\rangle$ in G_{36}, we may safely neglect the coupling to all other G_{36} states. Also the mixing of functions with different J gives a negligible contribution to the splitting. The expectation values of the dipole in the $G_2^\pm$ states with given parity are of course zero, but we find the following coupling between the states of different parity from Eq. (A8) in the Appendix

$$-\epsilon\langle i,G_2^\mp,JKM|\mu_0^{\text{SF}}|i,G_2^\pm,JKM\rangle$$

$$= -\epsilon\langle i,G,K|\mu_0^{\text{BF}}|i,G,K\rangle\langle JKM|D_{00}^{(1)*}|JKM\rangle$$

$$= -\frac{\epsilon\langle\mu\rangle_i KM}{J(J+1)}. \tag{3}$$

We took the space-fixed z-axis parallel to the static electric field ϵ, so we needed only the $m=0$ component of the dipole moment μ_m^{SF}. It is obvious from this equation that the off-diagonal dipole matrix element between the G_2^+ and G_2^- states of a given doublet is determined by the expectation value $\langle\mu\rangle_i = \langle i,G,K|\mu_0^{\text{BF}}|i,G,K\rangle$ of the (parallel) dipole of the corresponding G_{36} state. If one takes the zero-field splitting of the $G_2^\pm$ doublet from the far-infrared spectrum of Loeser
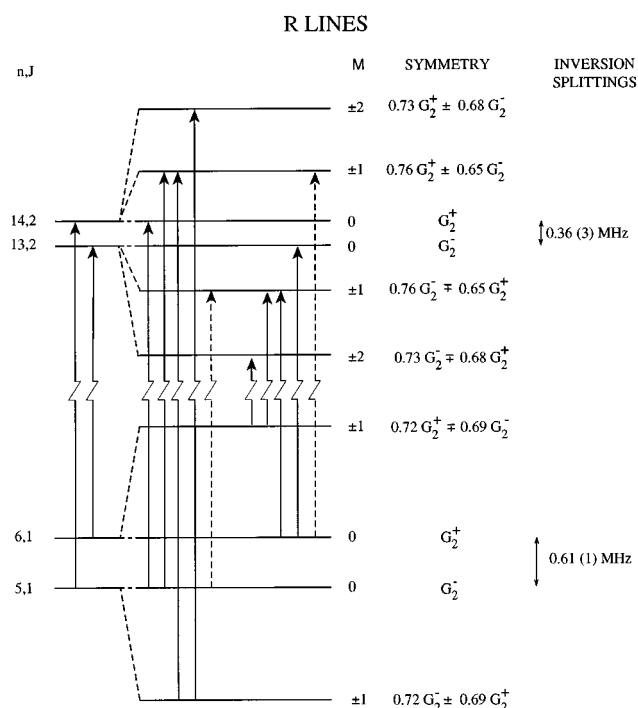
R LINES

FIG. 1. Energy level scheme of the $G:K=-1$ states for the observed R transitions, without (left) and with (right) applied electric field (40 V/cm). The arrows show the observed transitions, where the blended transitions (Table I) are indicated with dashed lines. The right-hand part of the figure shows the mixing of G_2^+ and G_2^- states in the levels for given M. The inversion splittings and their error estimates are taken from Ref. 8.
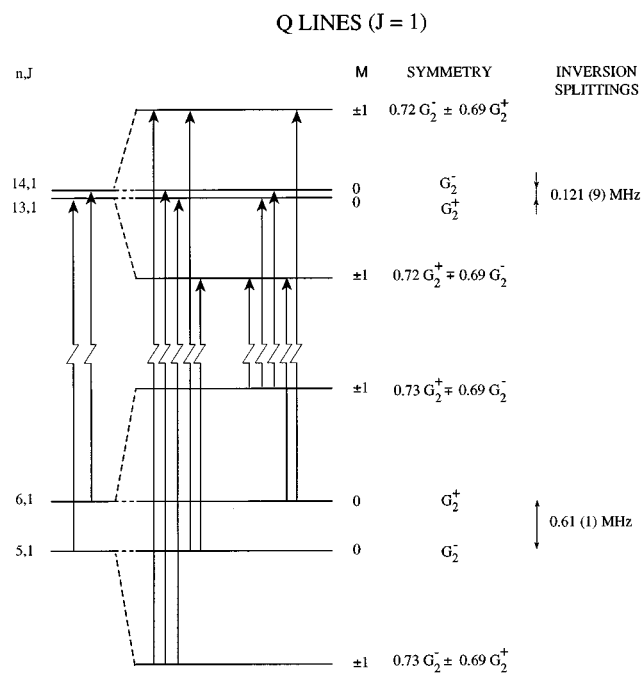
Q LINES $(J=1)$

FIG. 2. Energy level scheme for the $G:K=-1$ states for the observed Q transitions, without (left) and with (right) applied electric field (13.6 V/cm). The arrows show the observed transitions. The right-hand part of the figure shows the mixing of G_2^+ and G_2^- states in the levels for given M. The inversion splittings and their error estimates are taken from Ref. 8.

et al.[8] one may calculate the Stark splitting for a given (J,M) state in the usual way, i.e., by diagonalizing the matrix

$$
\begin{pmatrix}
E_{i,G_2^+} & \dfrac{-\epsilon\langle\mu\rangle_i KM}{J(J+1)} \\[2ex]
\dfrac{-\epsilon\langle\mu\rangle_i KM}{J(J+1)} & E_{i,G_2^-}
\end{pmatrix}.
\tag{4}
$$

The resulting splittings of the G state $i=0$, that corresponds to the $G_2^\pm$ states (5,6) of Ref. 8, and the G state $i=1$, i.e., the $G_2^\pm$ states (13,14), are shown in Figs. 1 and 2. For the selection rules discussed below it is important to remember that these states correspond to $K=-1$.

It is obvious from Eqs. (3) and (4) that the states with $M=0$ are not affected by the static electric field, so that the wave functions of these states remain purely G_2^+ and G_2^-. For all states with $M\neq0$ the off-diagonal electric field coupling matrix elements are substantially larger (for the field strengths used in the measurements) than the small zero-field splitting of the $G_2^\pm$ doublets. As shown in Figs. 1 and 2 the resulting states are therefore a nearly equal admixture of the G_2^+ and G_2^- states. Hence, these states have no longer a definite parity. The energy ordering of these perturbed levels is not determined by that of the unperturbed $G_2^\pm$ levels. Each perturbed state contains a slightly higher weight of the unperturbed G_2^+ or G_2^- state to which it is closest in energy, but

whether the plus or the minus combination of the G_2^+ and G_2^- states is highest depends only on the signs of M and K and on the sign of the permanent dipole moment $\langle\mu\rangle_i$ of the corresponding G state in G_{36}. The selection rules and intensities of the far-infrared transitions are strongly affected by this parity mixing.

C. Selection rules and intensities of infrared transitions

We will now discuss the far-infrared transitions between the Stark-split levels. From the general formula, Eq. (A8), for the dipole coupling matrix elements it follows that, as usually, transitions are allowed for $\Delta J=0$ (Q band) and for $\Delta J=\pm1$ (P and R bands) with $\Delta M=0$ or ±1. For the transitions between the G states of the ammonia dimer with $i=0$ and $i'=1$ (and the same $K=-1$) observed here, the transition dipole moment is given by

$$
\langle 1,G_2^\mp,J'KM'|\mu_m^{\mathrm{SF}}|0,G_2^\pm,JKM\rangle
$$
$$
=\mu_{01}\langle J'KM'|D_{m0}^{(1)*}|JKM\rangle
$$
$$
=\mu_{01}(-1)^{K-M'}[(2J'+1)(2J+1)]^{1/2}
$$
$$
\times\begin{pmatrix} J' & 1 & J \\ -M' & m & M \end{pmatrix}\begin{pmatrix} J' & 1 & J \\ -K & 0 & K \end{pmatrix},
\tag{5}
$$

where the internal factor $\mu_{01}=\langle1,G,K|\mu_0^{\mathrm{BF}}|0,G,K\rangle$ is the (parallel) transition dipole moment between the G states labeled (5,6) and those labeled (13,14). Since there is only this

TABLE I. Stark shifts for the observed transitions, n'' and n' label the vibrational-tunneling states according to Ref. 8. The * indicates those components that correlate to a forbidden zero-field transition. In the last column the calculated relative intensities of all the components with nonzero transition moment are reported.

Zero field transition $n',J',$symm.$\leftarrow n'',J'',$symm.	ν_0 (MHz)	Applied electric field (V/cm)	Obs. shifts (MHz)	$|M'|\leftarrow|M''|$	Calc. rel. intensities
$13,2,G_2^-\leftarrow 6,1,G_2^+$	767 195.53	40±1	0	0←0	4.0
			−1.026	1←0	2.3
			−8.299	1←1	3.0
			−9.601	2←1	7.9
			Not obs.	0←1	0.6
$13,2,G_2^-\leftarrow 5,1,G_2^-$		40±1	Partly blended	1←0*	1.6
			Not obs.	0←1*	0.6
$14,2,G_2^+\leftarrow 5,1,G_2^-$	767 196.53	40±1	0	0←0	4.0
			+1.021	1←0	2.3
			+8.370	1←1	3.0
			+9.646	2←1	7.9
			Not obs.	0←1	0.6
$14,2,G_2^+\leftarrow 6,1,G_2^+$		40±1	Partly blended	1←0*	1.6
			Not obs.	0←1*	0.6
$14,1,G_2^-\leftarrow 6,1,G_2^+$	747 019.13	13.6±0.3	+1.160	1←0	0.7
			−2.524	0←1	0.7
$13,1,G_2^+\leftarrow 6,1,G_2^+$		13.6±0.3	−1.360	1←0*	0.6
			−2.524	0←1*	0.6
			−3.706	1←1*	1.0
$13,1,G_2^+\leftarrow 5,1,G_2^-$	747 019.60	13.6±0.3	−1.160	1←0	0.7
			+2.538	0←1	0.7
$14,1,G_2^-\leftarrow 5,1,G_2^-$		13.6±0.3	+1.410	1←0*	0.6
			+2.538	0←1*	0.6
			+3.777	1←1*	1.0

single transition dipole moment μ_{01} occurring in all the observed transitions, while the rotational factors are essentially just products of $3j$ symbols, it is possible to calculate all the relative intensities of these transitions.

Here, we give the selection rules for the Q and R bands measured. As always, transitions between the levels with $M=0$ are forbidden in the Q band, but allowed in the R branch. Since the $M=0$ levels are not perturbed by the static field, these transitions obey the standard $+/-$ parity selection rules. But, transitions from $M=0$ to $M=\pm 1$ and vice versa are always allowed since the $M=0$ states are purely G_2^+ or G_2^-, while the $M=\pm 1$ states have nearly equal contributions of G_2^+ and G_2^- character. Transitions between the levels with $M=\pm 1$ and $M=\pm 2$ must obey the rule that $\Delta M=0$ or $\Delta M=\pm 1$. However, half of these transitions which are in principle allowed, are very weak. If we write the states with $M=\pm 1$ and ± 2 as $a|i,G_2^+\rangle+b|i,G_2^-\rangle$, see Figs. 1 and 2, the transition dipole moment is

$$\langle a'(i',G_2^+)+b'(i',G_2^-)|\mu_0^{SF}|a(i,G_2^+)+b(i,G_2^-)\rangle$$
$$=(a'b+ab')\langle i',G_2^+|\mu_0^{SF}|i,G_2^-\rangle. \qquad (6)$$

Since $|b'/a'|\approx|b/a|\approx 1$, it follows that the transition will be nearly forbidden if the sign of b'/a' differs from that of b/a (as it does in half of the cases).

One observes that especially the latter selection rules are rather specific for the ammonia dimer. They deviate from the standard selection rules for a (nearly) rigid rotor, in particular because all the levels involved are characterized by a single value of $K(=-1)$. We noted already that the energy ordering

of the $a|i,G_2^+\rangle+b|i,G_2^-\rangle$ combinations with positive and negative b/a is determined by the sign of the permanent dipole moment $\langle\mu\rangle_i$ of the corresponding G state. This by itself is not sufficient to experimentally determine the sign of this dipole moment $\langle\mu\rangle_i$, but in combination with the selection rules for the transitions between the levels with $M=\pm 1$ and $M=\pm 2$, it allows us to determine experimentally the *relative sign* of the dipole moments of the G states (5,6) and (13,14) involved in these transitions, see Sec. IV A.

IV. RESULTS

A. Experiment

We observed the Stark shifts and splittings in an electric field of the $R(1)$ transitions around 767 GHz and of the $Q(1)$ transitions around 747 GHz. All the observed transitions, with and without electric field, are indicated in Figs. 1 and 2. To label unambiguously the $M'\leftarrow M''$ components the lines that correlate to a $G_2^+\leftarrow G_2^+$ or $G_2^-\leftarrow G_2^-$ transition, i.e., to a forbidden zero-field transition, are marked by a star (*) in Table I. In an electric field several of these transitions become allowed because of parity mixing (see Sec. III C).

The relative intensities of the M components can be calculated from Eq. (5), taking into account the following two factors. In the first place, the ratio between perpendicular and parallel sideband power is about 2:3 (Sec. II), therefore the relative intensities of the $\Delta M=\pm 1$ and $\Delta M=0$ components scale with a factor of 0.66. Second, the mixing of the $G_2^\pm$ states by the electric field affects the transition dipole mo-
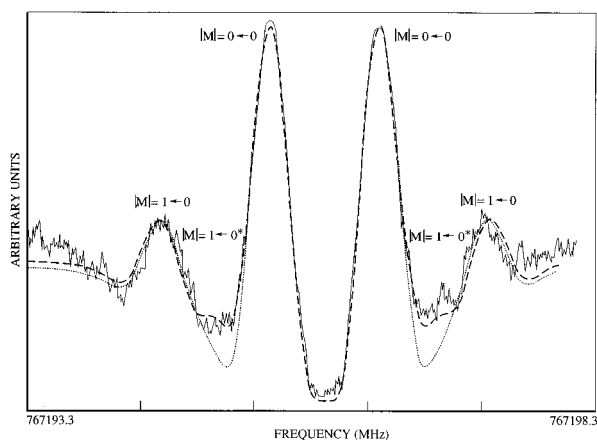
FIG. 3. Part of the Stark components of the $R(1)$ transitions recorded in a field of 40 V/cm. The solid line represents the experimental spectrum. The dotted line is the calculated spectrum without the $1\leftarrow0^*$ transition, while the dashed line includes the latter transition. The line shape used in the calculated spectrum is that of the second Fourier component of a Voigt profile, with the linewidth adjusted to match the experimental width (275 kHz half width at half maximum).

FIG. 4. The $Q(1)$ Stark spectrum recorded in a field of 13.6 V/cm.

ment through Eq. (6). Taking into account all these factors, we calculated the relative intensities of the Stark components as expected to be observed in this experiment. The results are reported in the last column of Table I.

For the $R(1)$ transitions we applied an electric field of 40 V/cm. Table I reports the Stark splittings. We observed two $\Delta M = 0$ and two $\Delta|M| = +1$ components for each of the two inversion transitions. The $\Delta|M| = -1$ transitions were not observed due to the low intensities (see Table I). The $1\leftarrow0^*$ transitions are predicted to fall just in between the $0\leftarrow0$ and the $1\leftarrow0$ transitions, and to show relatively low intensities (see Table I). A simulation of the spectrum using the calculated intensity ratio of the $1\leftarrow0^*$ and $1\leftarrow0$ transitions, see Table I, clearly demonstrates that the $1\leftarrow0^*$ transitions are indeed present in the experimental spectrum (see Fig. 3, dashed line). This nicely confirms the agreement between the experimental and calculated spectra, both for the frequencies and for the intensities. A comparison of the intensities of the $1\leftarrow1$ and the $2\leftarrow1$ transitions, which possess quite large Stark shifts, with those of the other components was hampered by the inhomogeneities in the electric field which tend to smear out the intensities. This was concluded from a comparison of measurements at 10 and 40 V/cm. Although the relative intensities of the low field spectrum are in much better agreement with the calculated ones, the lines could not fully be resolved, which prevented a good intensity comparison.

The $Q(1)$ transitions were observed in a field of 13.6 V/cm. Figure 4 shows the recorded spectrum, while Table I reports the Stark shifts. At 13.6 V/cm all the components are completely resolved, with the exception of the $0\leftarrow1$ and $0\leftarrow1^*$ components. The splitting of the latter two components does not depend on the applied electric field strength, but equals the inversion splitting in the excited interchange
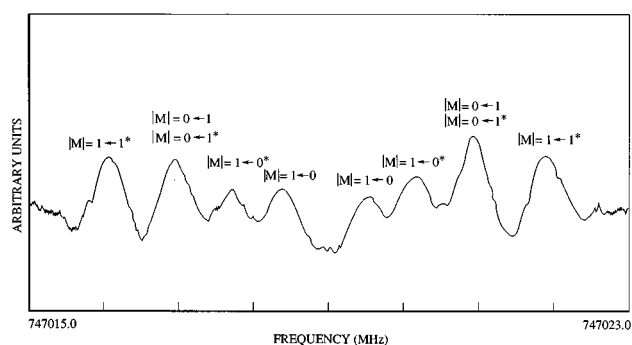
state (0.121 MHz) and cannot be resolved with the present experimental linewidth.

From the theory in Sec. III C it can be concluded, if the signs of the dipole moments for the upper and lower interchange states are equal, that the $1\leftarrow1$ transition is allowed, while the $1\leftarrow1^*$ transition is forbidden (actually very weak). On the other hand, if these signs are different, the $1\leftarrow1^*$ transition is allowed and the $1\leftarrow1$ transition is forbidden. From the experimental spectrum it is obvious that the $1\leftarrow1^*$ rather than the $1\leftarrow1$ Stark component has been observed. We therefore conclude that the two dipole moments have opposite signs.

Due to the absence of strong inhomogeneity effects in the electric field of 13.6 V/cm, it is also possible to perform a comparison between calculated and experimental intensities of the different Stark components. From Fig. 4 it follows that all $\Delta M = \pm1$ components have the same intensity, which is about 2/3 of that of the $\Delta M = 0$ transitions. This agrees very well with the calculated values from Table I.

In order to separate data for the upper and lower interchange levels we calculated combination differences between the observed transitions in such a way that pure Stark splittings in either the upper or lower interchange level were obtained. The result of this procedure is presented in Tables II and III. The electric dipole moments for the two states were then calculated by fitting them to the Hamiltonian of Eq. (4).

TABLE II. Differences in Stark shifts used in the fitting procedure (see the text) and comparison between observed and calculated splittings of the lower interchange level obtained from the fit. n'' and n' label the vibrational-tunneling states according to Ref. 8. The * indicates those components that correlate to a forbidden zero-field transition. The best fit value for $|\mu_{(5,6)}|$ is 0.763(15) D.

Type of splitting introduced in the fit		Observed splittings (MHz)	Calculated splittings (MHz)
Zero-field transition $n',J',\text{symm.}\leftarrow n'',J'',\text{symm.}$	Stark splitting		
$13,2,G_2^-\leftarrow6,1,G_2^+$	$(1\leftarrow1)-(1\leftarrow0)$	7.273	7.317
$14,2,G_2^+\leftarrow5,1,G_2^-$	$(1\leftarrow1)-(1\leftarrow0)$	7.349	7.317
$13,1,G_2^+\leftarrow6,1,G_2^+$	$(1\leftarrow1^*)-(1\leftarrow0^*)$	2.346	2.340
$14,1,G_2^-\leftarrow5,1,G_2^-$	$(1\leftarrow1^*)-(1\leftarrow0^*)$	2.367	2.340

TABLE III. Differences in Stark shifts used in the fitting procedure (see the text) and comparison between observed and calculated splittings of the excited interchange level obtained from the fit. n'' and n' label the vibrational-tunneling states according to Ref. 8. The * indicates those components that correlate to a forbidden zero-field transition. The best fit value for $|\mu_{(13,14)}|$ is 0.365(10) D.

Type of splitting introduced in the fit		Observed splittings (MHz)	Calculated splittings (MHz)
Zero-field transition	Stark splitting		
$13,2,G_2^- \leftarrow 6,1,G_2^+$	$(1\leftarrow0)-(0\leftarrow0)$	1.026	1.062
	$(2\leftarrow1)-(1\leftarrow1)$	1.302	1.262
$14,2,G_2^+ \leftarrow 5,1,G_2^-$	$(1\leftarrow0)-(0\leftarrow0)$	1.021	1.062
	$(2\leftarrow1)-(1\leftarrow1)$	1.276	1.262
$13,1,G_2^+ \leftarrow 6,1,G_2^+$	$(1\leftarrow1^*)-(1\leftarrow0^*)$	1.182	1.180
$14,1,G_2^- \leftarrow 6,1,G_2^+$	$(1\leftarrow0)-(0\leftarrow0)$	1.160	1.180
$14,1,G_2^- \leftarrow 5,1,G_2^-$	$(1\leftarrow1^*)-(1\leftarrow0^*)$	1.179	1.180
$13,1,G_2^+ \leftarrow 5,1,G_2^-$	$(1\leftarrow0)-(0\leftarrow0)$	1.160	1.180

TABLE IV. Dipole moments of $(NH_3)_2$ in the lowest G states.

State labels[a]	Calculated	Experiment
	$K=0$	
(1,2)	-0.66 D[b]	0.74 D[c]
(11,12)	0.50 D[b]	
	$K=1$	
(3,4)	0.19 D[b]	0.10 D[d]
(9,10)	-0.12 D[b]	<0.09 D[d]
	$K=-1$	
(5,6)	-0.74 D[e]	-0.763 D[e]
(13,14)	0.35 D[e]	0.365 D[e]

[a]The states are labeled as in Ref. 8.
[b]From Ref. 3.
[c]From Refs. 6 and 7, only the absolute value has been measured.
[d]From Ref. 14, only the absolute value has been measured.
[e]Present paper.

Tables II and III list the results of the least squares fit. The experimental error associated with the splittings is 50 kHz. The resulting ground state (5,6) electric dipole moment value is 0.763(15) D, while for the excited interchange state (13,14) a value of 0.365(10) D is found. As concluded above, these dipole moments have opposite signs. The main contribution to the uncertainties in the dipole moments originates from the error in the applied electric field. The frequency errors in the inversion splittings ($E_{G_2^+} - E_{G_2^-}$), which occur in Eq. (4) and enter into the analysis, play a minor role. Since the uncertainty in the applied electric field affects all the measurements in the same way, the *ratio* between the dipole moments of the two states is more accurate: it is found to be $-2.09(1)$.

B. Theoretically calculated dipole moments

Using the G state wave functions obtained from the semiempirical potential in Ref. 3 and the dipole operator in Eq. (A2), we have calculated the permanent dipole moments of the G states observed here. The Hamiltonian, the basis and the computational procedure are the same as described in Ref. 3. For the states (5,6) this yields a dipole moment of -0.74 D, for the states (13,14) a value of $+0.35$ D. In defining the overall sign of the dipole moments of the G states we use the convention of Ref. 2 that A is the ortho monomer and B is the para monomer, while the positive z axis points from A to B. This is consistent with the sign of the dipole moments and the values of the nuclear quadrupole splittings given in Ref. 3.

V. CONCLUSION

We have analyzed the effects of an electric field on the $R(1)$ and $Q(1)$ transitions between the VRT states $G:K=-1$ of the ammonia dimer: $(5,6)\rightarrow(13,14)$, band origin 747.2 GHz. The dipole moments of both states are determined. The theoretically calculated values agree very well with the experimental ones. Because of the very small zero-field splittings between the $G_2^\pm$ levels, the high field limit is easily

reached, so that the parity of the energy levels with $M\neq0$ is no longer defined. The appropriate selection rules for the Stark components have been derived, which not only allowed us to explain the unexpected Stark pattern, but also to determine experimentally that the signs of $\mu_{(5,6)}$ and $\mu_{(13,14)}$ are different. From theoretical calculations we find a negative value for $\mu_{(5,6)}$ and a positive value for $\mu_{(13,14)}$. The results are summarized in Table IV, together with the dipole moments of other G states measured and/or calculated previously.

The negative dipole moment implies that in the lowest G state with $K=-1$, which corresponds to the $G_2^\pm$ levels (5,6), the para monomer is the proton donor and the ortho monomer is the proton acceptor. The opposite sign of the dipole moment in the first excited G state with $K=-1$, i.e., the levels (13,14), indicates that the donor/acceptor roles of the ortho and para monomers are reversed upon excitation. The same reversal upon excitation follows from calculations[3] for the G states with $K=0$, i.e., the levels (1,2) and (11,12), and for those with $K=1$, i.e., the levels (3,4) and (9,10). The ground state dipole is negative also for $G:K=0$, but not for $G:K=1$. However, in the latter case its absolute value is considerably smaller.

Another property of $(NH_3)_2$ which has been found (see Table IV), is that for all these G states the absolute value of the dipole moment becomes smaller upon excitation, in other words, that the average structure becomes more nearly cyclic. More in general, it should be noted that the average structure is rather different from a classical hydrogen bonded structure, so that the roles of proton donor and acceptor should not be interpreted too strictly; they apply only in a relative sense. Moreover, the average structure is the result of averaging over large amplitude motions, which occur especially along the interchange path (see Ref. 3) with its very low barrier of about 7 cm^{-1}. The fact that the absolute value of the average dipole moment is smaller in the excited G states (for each K) leads to the conclusion that the vibrational amplitude has increased, i.e., that the average structure is even more different from the (noncyclic) equilibrium structure than in the ground states.

ACKNOWLEDGMENTS

APPENDIX: DIPOLE MATRIX ELEMENTS

In this Appendix we derive a general expression for the dipole coupling matrix elements between the states of the ammonia dimer with inverting monomers, with the wave functions given by Eq. (1). From this derivation it follows how these matrix elements between the states of the dimer adapted to the full symmetry group G_{144} are related to the permanent dipole of the van der Waals states of the dimer with rigid monomers, adapted to the subgroup G_{36}, and to the transition dipole moments between the latter states.

We start with an expression for the dipole operator similar to that used in Refs. 2 and 3, but since we wish to consider the umbrella inversion of the ammonia monomers, we have now included explicitly the dependence of the dipole operator on the umbrella angles ρ_A and ρ_B. The spherical components μ_m of the dipole relative to an arbitrary space-fixed or laboratory frame can be expressed as follows:[18]

$$\mu_m^{\mathrm{SF}} = \sum_k \mu_k^{\mathrm{BF}} D_{mk}^{(1)}(\alpha, \beta, 0)^*. \tag{A1}$$

The components μ_k^{BF} are the components relative to the body-fixed frame with its z axis along $\mathbf{R}$ that was used in Refs. 2, 3, and 13. The angles α and β are the polar angles of $\mathbf{R}$ in the laboratory frame. Actually we need only the parallel component μ_k^{BF} with $k=0$, because we do not consider perpendicular $\Delta K = \pm 1$ transitions in this paper. For this parallel component we write the following expression:

$$\mu_a = \mu_0^{\mathrm{BF}} = [\mu(\rho_A) \cos \theta_A + \mu(\rho_B) \cos \theta_B](1 + 2\alpha_0 R^{-3}). \tag{A2}$$

The angles θ_A and θ_B are the angles between the C_3 axes of the ammonia monomers and the vector $\mathbf{R}$. The umbrella angles ρ_A and ρ_B, which range from 0 to π and are equal to $\pi/2$ for a flat ammonia monomer, are defined as the angles between the N–H bonds of a monomer and its C_3 axis. This expression is an approximate one; it includes only the permanent monomer dipole moments and the dipole–induced dipole moments. It is assumed that the ammonia monomers retain C_{3v} symmetry, so that their dipoles remain parallel to their C_3 axes and that the dipole polarizability α_0 of the monomers is isotropic (this is nearly true[19]). We need not consider the umbrella angle dependence of α_0, since we will only use umbrella wave functions $f_\pm(\rho_A)$ and $f_\pm(\rho_B)$ for the monomers that are localized near the equilibrium values of ρ_A and ρ_B and the polarizability α_0 is the same for both equilibrium structures of the umbrellas, up or down.

For the monomer dipole expectation values we may write, for $X = A$ or B,

$$\mu_X = \langle f_+(\rho_X) | \mu(\rho_X) | f_+(\rho_X) \rangle$$
$$= -\langle f_+(\rho_X) | \mu(\pi - \rho_X) | f_+(\rho_X) \rangle$$
$$= -\langle f_-(\rho_X) | \mu(\rho_X) | f_-(\rho_X) \rangle$$
$$= \langle f_-(\rho_X) | \mu(\pi - \rho_X) | f_-(\rho_X) \rangle \tag{A3}$$

since the umbrella functions are related as $f_+(\rho_X) = f_-(\pi - \rho_X)$. Because these functions are localized near one of the minima of the NH_3 double-well potential and have negligible overlap, we may also assume that all off-diagonal dipole matrix elements are negligible

$$\langle f_+(\rho_X) | \mu(\rho_X) | f_-(\rho_X) \rangle = 0. \tag{A4}$$

Note that this is consistent with the relation between these localized up/down umbrella functions and the even/odd umbrella inversion eigenstates $\psi^\pm(\rho_X)$ of the ammonia monomer $f_\pm(\rho_X) = [\psi^+(\rho_X) \pm \psi^-(\rho_X)]/\sqrt{2}$, see Ref. 13. Equations (A3) and (A4) are equivalent to the fact that the even/odd eigenstates $\psi^\pm$ have a vanishing dipole expectation value, while the "dipole moment" μ_X of the NH_3 molecule is the off-diagonal element $\langle \psi^+(\rho_X) | \mu(\rho_X) | \psi^-(\rho_X) \rangle$.

We now consider the dipole matrix elements between the states i and i' of different parity adapted to G_{144}, with wave functions given by Eq. (1)

$$\langle i', G_2^{\mp}, J'K'M' | \mu_m^{\mathrm{SF}} | i, G_2^{\pm}, JKM \rangle$$
$$= \tfrac{1}{4} \langle ++ | \langle J'K'M' | \langle i', G, K' | (E \mp E^*)[E - (23)]$$
$$\mu_m^{\mathrm{SF}}[E - (23)](E \pm E^*) | i, G, K \rangle | JKM \rangle | ++ \rangle. \tag{A5}$$

The components μ_m^{SF} of the dipole operator must be invariant under all permutations and change sign under E^* and, therefore, transform as

$$(23)\mu_m^{\mathrm{SF}}(23) = \mu_m^{\mathrm{SF}},$$
$$E^* \mu_m^{\mathrm{SF}} E^* = -\mu_m^{\mathrm{SF}}. \tag{A6}$$

These relations lead to the following simplification in Eq. (A5):

$$\tfrac{1}{4}(E \mp E^*)[E - (23)]\mu_m^{\mathrm{SF}}(E \pm E^*)[E - (23)]$$
$$= \mu_m^{\mathrm{SF}}(E \pm E^*)[E - (23)]. \tag{A7}$$

Because $(23)|++\rangle = |-+\rangle$ and $E^*|++\rangle = |--\rangle$ and the off-diagonal matrix elements of the monomer dipole operators $\mu(\rho_X)$ between the localized functions $f_+(\rho_X)$ and $f_-(\rho_X)$ may be neglected, we further note that only the identity operator E has a nonvanishing contribution to Eq. (A5). We may then rewrite Eq. (A5) as

$$\langle i', G_2^{\mp}, J'K'M' | \mu_m^{\mathrm{SF}} | i, G_2^{\pm}, JKM \rangle$$
$$= \delta_{K'K} \langle i', G, K | \mu_0^{\mathrm{BF}} | i, G, K \rangle \langle J'KM' | D_{m0}^{(1)*} | JKM \rangle, \tag{A8}$$

where in μ_0^{BF} we have replaced the monomer operators $\mu(\rho_A)$ and $\mu(\rho_B)$ by their expectation values μ_A and μ_B over $f_+(\rho_A)$ and $f_+(\rho_B)$. This result can be used to derive the Stark splitting of the VRT states of the ammonia dimer, as well as to derive the intensities of the allowed far-infrared transitions.

[1] D. D. Nelson, G. T. Fraser, and W. Klemperer, Science **238**, 1670 (1988).

[2] J. W. I. van Bladel, A. van der Avoird, P. E. S. Wormer, and R. J. Saykally, J. Chem. Phys. **97**, 4750 (1992).

[3] E. H. T. Olthof, A. van der Avoird, and P. E. S. Wormer, J. Chem. Phys. **101**, 8430 (1994).

[4] H. Linnartz, M. Havenith, and W. L. Meerts, CAMP **30**, 315 (1995).

[5] A. van der Avoird, G. T. Fraser, M. Havenith, W. Klemperer, H. Linnartz, J. G. Loeser, W. L. Meerts, D. D. Nelson, E. H. T. Olthof, R. J. Saykally, W. Stahl, and P. E. S. Wormer, Science (in preparation).

[6] D. D. Nelson, G. T. Fraser, and W. Klemperer, J. Chem. Phys. **83**, 6201 (1985).

[7] D. D. Nelson, W. Klemperer, G. T. Fraser, F. J. Lovas, and R. D. Suenram, J. Chem. Phys. **87**, 6364 (1987).

[8] J. G. Loeser, C. A. Schmuttenmaer, R. C. Cohen, M. J. Elrod, D. W. Steyert, R. J. Saykally, R. E. Bumgarner, and G. A. Blake, J. Chem. Phys. **97**, 4727 (1992).

[9] M. Havenith, H. Linnartz, E. Zwart, A. Kips, J. J. ter Meulen, and W. L. Meerts, Chem. Phys. Lett. **193**, 261 (1992).

[10] H. Linnartz, W. L. Meerts, and M. Havenith, Chem. Phys. **193**, 327 (1995).

[11] E. H. T. Olthof, A. van der Avoird, and P. E. S. Wormer, J. Mol. Struct. (Theochem) **307**, 201 (1994).

[12] A. van der Avoird, E. H. T. Olthof, and P. E. S. Wormer, Faraday Discuss. Chem. Soc. **97**, 43 (1994).

[13] E. H. T. Olthof, A. van der Avoird, P. E. S. Wormer, J. G. Loeser, and R. J. Saykally, J. Chem. Phys. **101**, 8443 (1994).

[14] H. Linnartz, A. Kips, W. L. Meerts, and M. Havenith, J. Chem. Phys. **99**, 2449 (1993).

[15] S. X. Wang, J. L. Booth, F. W. Dalby, and I. Ozier, J. Chem. Phys. **101**, 5464 (1994).

[16] P. Verhoeve, E. Zwart, M. Versluis, M. Drabbels, J. J. ter Meulen, W. L. Meerts, A. Dymanus, and D. B. McClay, Rev. Sci. Instrum. **61**, 1612 (1990).

[17] D. M. Brink and G. R. Satchler, *Angular Momentum* (Clarendon, Oxford, 1975).

[18] A. van der Avoird, P. E. S. Wormer, and R. Moszynski, Chem. Rev. **94**, 1931 (1994).

[19] P. E. S. Wormer and H. Hettema, J. Chem. Phys. **97**, 5592 (1992).